

Pressure-induced anomalous enhancement in superconducting critical temperature of transition-metal chalcogenide Ta₂PdS₆ and Ta₂PdSe₆

**Ryo Matsumoto¹, Akitoshi Nakano³, Takafumi D Yamamoto⁴, Kensei Terashima¹, Kazuki Yamane^{1,2}, Masahiro Ohkuma¹, Ichiro Terasaki³, Yoshihiko Takano^{1,2}*

¹Research Center for Materials Nanoarchitectonics (MANA),

National Institute for Materials Science, Tsukuba, Ibaraki 305-0047, Japan

²Graduate School of Pure and Applied Sciences, University of Tsukuba, Tsukuba, Ibaraki 305-8577, Japan

³Department of Physics, Nagoya University, Nagoya 464-8602, Japan

⁴Department of Material Science and Technology, Tokyo University of Science, Tokyo 125-8585, Japan

**Corresponding author; Email: MATSUMOTO.Ryo@nims.go.jp*

Abstract

The emergence of a second dome in the superconducting phase through pressure-driven manipulation of crystal structures in materials has attracted considerable attention. Transition metal chalcogenides (TMCs) represent a highly promising platform, as the second dome has been observed in several binary compounds. Recently, ternary TMCs such as Ta₂PdS₆ and Ta₂PdSe₆ have exhibited pressure-induced superconducting domes. In this study, we perform electrical transport measurements of Ta₂PdS₆ and Ta₂PdSe₆ under extremely high pressures exceeding 100 GPa, namely uninvestigated regions in previous reports, to reveal the emergence of the second dome. The superconducting critical temperatures (T_c) in both Ta₂PdS₆ and Ta₂PdSe₆ initially decrease with increasing pressure. Subsequently, the T_c s tend to enhance drastically above 100 GPa. Notably, the maximum T_c in Ta₂PdS₆ is 11.2 K at 130.0 GPa, which is a relatively high record among the TMCs. The emergence of the second dome in Ta₂PdS₆ and Ta₂PdSe₆ opens further motivation for the investigation under extreme conditions beyond the first dome to find hidden ordered phases.

1. Introduction

Application of high pressure is an effective method to tune the structural and electronic properties of materials. In particular, the effects of pressure on the emergence and suppression of ordered phases, such as charge density wave (CDW), spin density wave (SDW), and superconductivity (SC), have attracted significant research attention in recent decades [1–6]. The transition temperatures of these ordered phases typically exhibit a dome-like behavior under applied pressure. Interestingly, the emergence of a second SC phase is observed in several materials following the suppression of the first SC dome [7]. Although most second SC domes show a lower or comparable T_c than that of the first SC dome, certain compounds, such as the ion-based superconductors, exhibit higher T_c in the second dome [8,9]. The reemergent superconductivity with a higher T_c in the second dome of other material families has become a focused research area, as theoretical calculations have predicted in high- T_c materials [10].

Transition metal chalcogenides (TMCs) have been focused as the platform for studying dome-like behavior in ordered phases under high pressure, particularly in binary systems, such as a pressure-driven suppression of the CDW phase and the emergence of SC phase [11–13]. Recently, ternary TMCs of Ta_2PdS_6 and Ta_2PdSe_6 , which crystallize in a monoclinic quasi-1D structure with space group $C2/m$, as shown in Fig. S1, have been studied actively due to their anomalous electrical properties at ambient pressure. For instance, Ta_2PdS_6 exhibits semiconducting behavior with an electron carrier density of $4.6 \times 10^{18} \text{ cm}^{-3}$ at 100 K [14], despite band calculations predicting a metallic state in the electronic structure. The transport measurements of the semimetal Ta_2PdSe_6 reveal a non-Fermi liquid-like temperature dependence, indicating an exotic electronic state with an unconventional scattering process for charge carriers [15]. Among the investigations of fundamental physics in this system, the emergence of the SC phase through the application of pressure has been reported in both Ta_2PdS_6 and Ta_2PdSe_6 , with dome-like behavior of T_c [16,17]. However, the question of reemergent SC phases beyond the first dome in this system remains an open issue.

In this study, we perform electrical transport measurements on single-crystalline Ta_2PdS_6 and Ta_2PdSe_6 under extremely high pressures to investigate the SC properties beyond the first dome. Through the electrical resistance measurements on Ta_2PdS_6 and Ta_2PdSe_6 above the megabar pressure range, we reveal the existence of a second SC phase with a T_c higher than that in the first dome. Specifically, the T_c in Ta_2PdS_6 rises drastically above 80.4 GPa, reaching 11.2 K at 130.0 GPa. This observation of the second SC dome with a higher T_c under extreme pressure offers significant motivation to investigate the megabar pressure region in functional materials, potentially opening new aspects of materials physics.

2. Materials and methods

High-quality single crystals of Ta_2PdS_6 and Ta_2PdSe_6 were grown for electrical transport

measurements and Raman spectroscopy under high pressure using a chemical vapor transport with a transport agent of I_2 by referring to previous reports [14,18,19]. Starting materials of tantalum (99.9%), palladium (99.9%), and sulfur (99.999%) or selenium (99.9% or 99.999%) were loaded into an evacuated quartz tube with an I_2 concentration of $\sim 3 \text{ mg cm}^{-3}$. A temperature difference of 145°C between 875 and 730°C in a three-zone furnace facilitated crystal growth over four days. The compositional ratio is evaluated by energy dispersive spectrometry (EDX) using a JSM-6010LA (JEOL). Details of the characterization of the obtained sample at ambient pressure were provided elsewhere [14]. A polycrystalline sample of Ta_2PdS_6 was synthesized via a solid-state reaction for a structural analysis under high pressure. The same starting powders as the single crystalline sample were used. The raw powder, once heated to 550°C , was re-grounded and heated at 730°C for 48 h in a tube furnace. The obtained sample was identified as a single phase of Ta_2PdS_6 by powder X-ray diffraction (XRD). The crystal structure was displayed by VESTA software [20].

Electrical transport measurements under high pressure in Ta_2PdS_6 and Ta_2PdSe_6 were conducted within a diamond anvil cell (DAC), employing a diamond electrode [21–23]. The temperature (T) dependence of resistance (R) was measured in the physical property measurement system (PPMS, Quantum Design) with a superconducting magnet. Raman spectroscopy was also performed at room temperature for the sample to evaluate the vibrational modes under high pressure. The diamond anvil equipped a beveled culet with a diameter of $\sim 100 \mu\text{m}$. A cleaved single-crystalline sample was positioned onto the diamond anvil with the electrodes, and a SUS316 plate served as a metal gasket. The pressure-transmitting medium and insulating layer consisted of cubic BN powders. The applied pressure was estimated using fluorescence from ruby powder placed on the culet [24] and the Raman spectrum from the diamond anvil itself [25], employing an inVia Raman Microscope (RENISHAW).

The crystal structure of Ta_2PdS_6 under high pressure was investigated through XRD measurements in the DAC. The culet of diamond anvil was $300 \mu\text{m}$, the gasket was a tungsten plate, and the PTM was the sample itself. These measurements were carried out using synchrotron radiation at the AR-NE1A beamline of the Photon Factory (PF) located at the High Energy Accelerator Research Organization (KEK). The X-ray beam monochromatized to an energy of 30 keV ($\lambda = 0.4175 \text{ \AA}$), was directed to the sample in the DAC through a collimator with a diameter of $50 \mu\text{m}$. The obtained XRD patterns were integrated into a one-dimensional profile using IPAnalyzer [26]. The applied pressure was estimated using the same procedures as those used for electrical measurements.

3. Results and discussion

Figure 1 shows the R - T characteristics of Ta_2PdS_6 under various pressures up to (a) 25.6 GPa , (b) 130.0 GPa , and (c) enlarged plots at low temperatures. The behavior of Ta_2PdS_6 under pressure is divided into three regions: (i) suppression of semiconducting behavior and transition to metallic

property below 21.5 GPa, (ii) emergence of SC phase at 25.6 GPa with a gradual change in T_c up to 70.0 GPa, and (iii) a drastic enhancement in T_c above 80.4 GPa. In region (i), Ta_2PdS_6 exhibits semiconducting characteristics, with a negative dR/dT at low temperatures under the lowest pressure of 1.4 GPa. This semiconducting curve is gradually suppressed with increasing pressure up to 18.6 GPa. Conversely, the R - T properties show metallic behavior across the measured temperature range at 21.5 GPa, indicating a semiconductor-to-metal transition. According to in-situ XRD analysis and Raman spectroscopy under pressure (Fig. S2), this metallization is due to a pressure-induced isosymmetric structural transition in Ta_2PdS_6 [17]. In region (ii), a sharp decrease in R , corresponding to the emergence of SC phase, appears above 25.6 GPa. The R starts to drop from 6.5 K, defined as T_c^{onset} , and gradually decreases to zero with several kinks, indicating inhomogeneous superconductivity. At 58.9 GPa, R reaches zero at T_c^{zero} of 2.5 K, with only slight changes in T_c as pressure increases up to 70.0 GPa. In this SC region, a sign reversal in Hall resistivity is reported in both Ta_2PdSe_6 [16] and Ta_2PdS_6 [17]. However, in our observation for Ta_2PdS_6 , a negative slope in Hall resistance, due to electron carriers, is dominant even at the lowest pressure and maintained up to SC region, as indicated in Fig. S3. Notably, T_c increases sharply under further compression above 80.4 GPa, corresponding to region (iii). Although the rate of increase in T_c slows above 100.3 GPa, the enhancement does not fully saturate even at the highest pressure, reaching maximum values of 11.2 K for T_c^{onset} and 8.5 K for T_c^{zero} at 130.0 GPa, marking a relatively high T_c among TMCs.

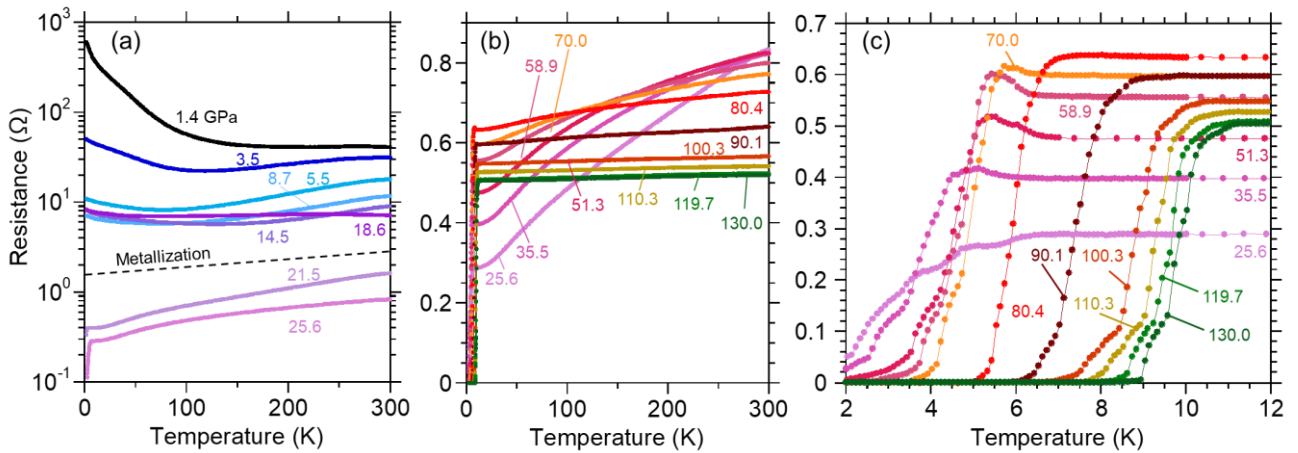


Fig. 1. (a) Temperature dependence of resistance under various pressures from 1.4 to 25.6 GPa and (b) 25.6 to 130.0 GPa in Ta_2PdS_6 . (c) Enlarged plots around superconducting transition.

Figure 2 presents the R - T properties of Ta_2PdSe_6 under pressures up to (a) 60.5 GPa, (b) 118.8 GPa, and (c) enlarged plots at low temperatures. The behavior of Ta_2PdSe_6 under pressure is also divided into two regions: (i) emergence of pressure-induced SC at 16.9 GPa and gradual change in T_c up to 92.1 GPa, and (ii) drastic enhancement in T_c above 102.1 GPa. In contrast to Ta_2PdS_6 , Ta_2PdSe_6 exhibits metallic behavior even at low pressures, and its SC phase appears at a lower pressure of 16.9 GPa. The SC transition is initially broad at 16.9 GPa due to pressure inhomogeneity. With applying

pressure, T_c^{onset} decreases gradually, and the SC transition becomes sharp, with zero resistance achieved above 60.5 GPa. With further compression, T_c^{onset} shows a slight increase up to 102.1 GPa. A drastic rise in T_c^{onset} above 102.1 GPa indicates the emergence of a second dome of pressure-induced SC in Ta₂PdSe₆.

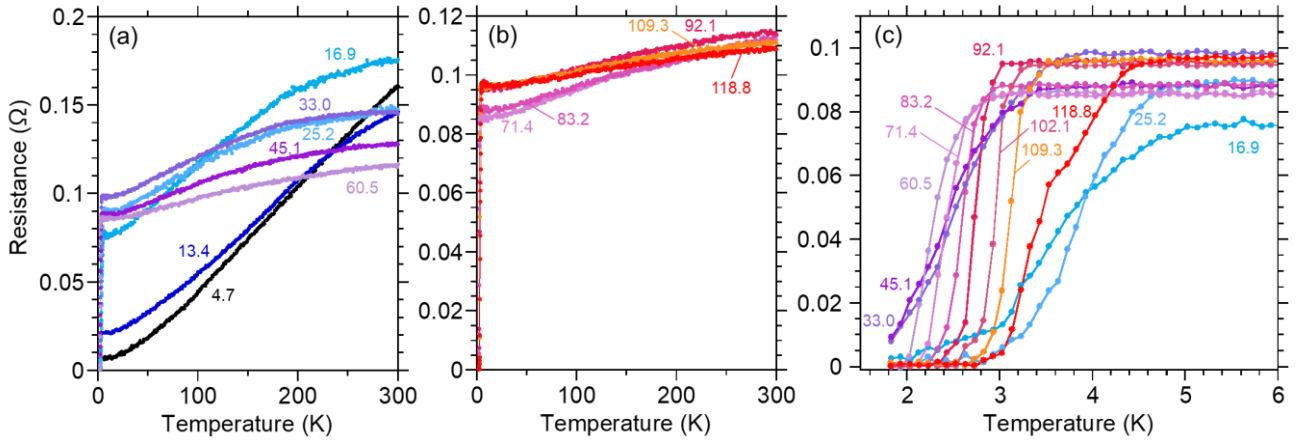


Fig. 2. (a) Temperature dependence of resistance under various pressures from 4.7 to 60.5 GPa and (b) 71.4 to 118.8 GPa in Ta₂PdSe₆. (c) Enlarged plots around superconducting transition.

Figure 3 presents the pressure-dependent T_c^{onset} in Ta₂PdS₆ and Ta₂PdSe₆ up to the megabar region, with comparisons to previous reports. In the unexplored pressure range beyond previous studies on Ta₂PdS₆ and Ta₂PdSe₆, specifically above the megabar region, our samples show a significant enhancement of T_c , revealing the existence of the second SC dome. Even at the maximum pressures in this study, the increases in T_c are not fully saturated. In contrast to most two-dome SC systems, where the second dome exhibits a lower or comparable T_c (e.g., CsV₃Sb₅ [7]), Ta₂PdS₆ shows double T_c of 11.2 K at 130.0 GPa than that observed at 70.0 GPa. Similarly, T_c in Ta₂PdSe₆ at 118.8 GPa is comparable to that at 16.9 GPa and continues to enhance steeply with applying pressure. The observed higher T_c s in the second SC domes are unique features in these materials. Although the behavior of Ta₂PdS₆ in low-pressure region differs from the previous report [17], a possible reason is slight changes in the composition. In the previous report, the composition was Ta:Pd:S = 1.9 : 1 : 5.7 with a p-type carrier [17], whereas our sample is Ta:Pd:S = 2.0 : 1 : 5.7 with an n-type carrier as shown by Hall measurement (Fig. S3). The slight difference may induce the distinct behavior at lower pressures, as metal vacancies introduce p-type doping in several TMCs [32,33].

This drastic enhancement of T_c under high pressure is unusual, as the application of pressure typically decreases T_c due to phonon hardening and a reduction in the electronic density of state (DOS) at Fermi energy, based on Bardeen–Cooper–Schrieffer (BCS) theory [27,28]. Two-dome behavior of T_c is typically associated with structural phase transitions, as seen in FeS [29], LaFeAsO_{1-x}F_x [30], and other compounds [31]. However, a recently discovered SC phase in the topological kagome metal CsV₃Sb₅ shows two-dome T_c attributed to a pressure-induced Lifshitz transition, resulting from a

reconstruction of the Fermi surface without structural phase transition [7]. The elevated T_c in Ta_2PdS_6 and Ta_2PdSe_6 likely relate to a modification of electronic structure rather than a structural phase transition, as discussed later.

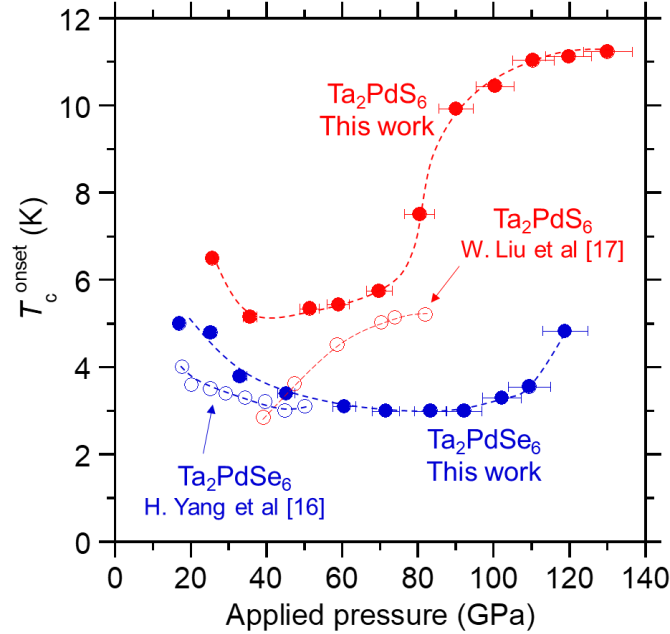


Fig. 3 Pressure-dependent T_c in Ta_2PdS_6 and Ta_2PdSe_6 up to megabar region with a comparison of previously reported data of Ta_2PdS_6 [17] and Ta_2PdSe_6 [16]. The dashed lines are the guide for the eyes.

To discuss the origin of anomalous enhancements, the pressure dependence of R at 300 K ($R_{300\text{K}}$) in both compounds is plotted in Fig. 4 (a). In Ta_2PdS_6 , $R_{300\text{K}}$ decreases monotonically with increasing pressure and reduces discretely at 21.5 GPa near P_c , suggesting a first-order transition. $R_{300\text{K}}$ gradually decreases further above 25.6 GPa until the maximum pressure of 130.0 GPa, without any additional discrete shifts. Similar gradual changes in $R_{300\text{K}}$ are observed in Ta_2PdSe_6 . Figure 4 (b) plots the pressure dependence of the upper critical field $\mu_0 H_{c2}(0)$ and coherence length at zero temperature $\xi(0)$ in Ta_2PdS_6 and Ta_2PdSe_6 . To estimate these parameters, R - T curves under various magnetic fields were fitted with the Werthamer-Helfand-Hohenberg (WHH) model [34,35] using a T_c criterion at 95% of the normal resistance (Fig. S4). The maximum $\mu_0 H_{c2}(0)$ is 11.3 T at 130.0 GPa in Ta_2PdS_6 and 3.5 T at 109.35 GPa in Ta_2PdSe_6 . These values are lower than the weak-coupling Pauli limit ($1.84T_c$), suggesting the absence of the Pauli paramagnetic pair-breaking effect. The $\xi(0)$ was derived from the Ginzburg-Landau (GL) formula $\mu_0 H_{c2}(0) = \Phi_0/2\pi\xi(0)^2$, where Φ_0 is the fluxoid. The smooth changes in $R_{300\text{K}}$, $\mu_0 H_{c2}(0)$, and $\xi(0)$ as pressure increases beyond P_c suggest that the origin of the second SC dome is linked to modifications in electronic structures, such as a Lifshitz transition, as seen in kagome metal [7]. First-principles calculations on Ta_2PdS_6 indicate that enhanced DOS at Fermi energy plays a crucial role in the emergence of SC phase [17]. The observed T_c enhancement is possibly associated

with DOS peaks near Fermi energy, which is a favorable condition for superconductivity, as seen in high- T_c hydrides [36]. Our finding of the hidden SC phase in Ta_2PdS_6 and Ta_2PdSe_6 reveals the importance of exploring extreme conditions to accelerate further development of materials physics.

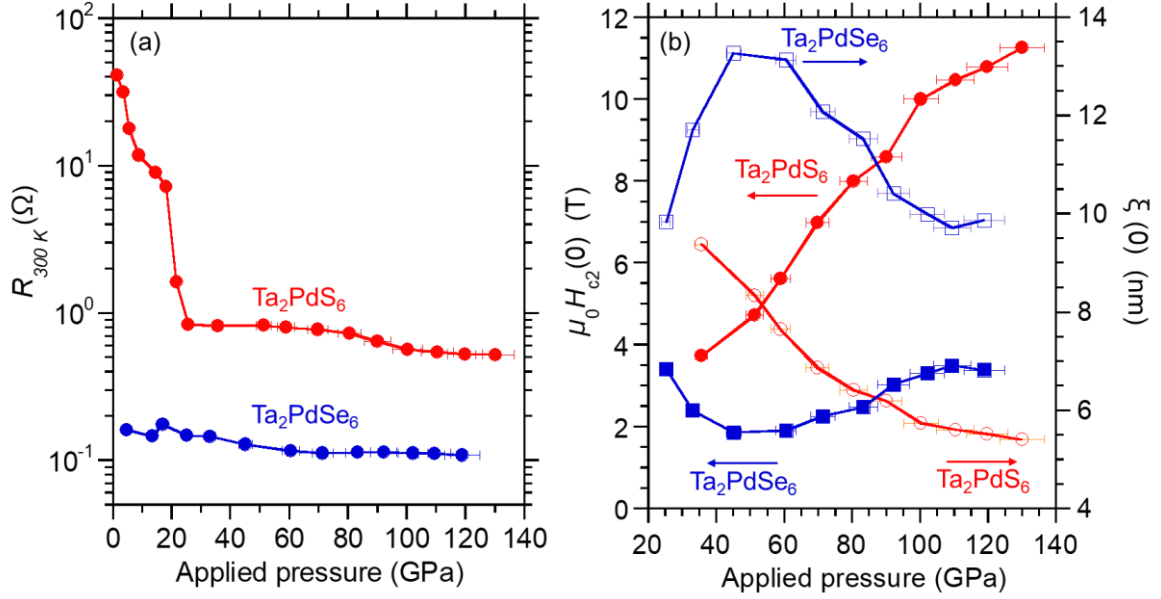


Fig. 4 (a) Pressure-dependent resistance at 300 K, (b) $\mu_0 H_{c2}(0)$, and $\xi(0)$ in Ta_2PdS_6 and Ta_2PdSe_6 .

4. Conclusion

In this study, we conduct the electrical transport measurements under high pressure up to 130.0 GPa in Ta_2PdS_6 and 118.8 GPa in Ta_2PdSe_6 to investigate SC properties beyond the first dome. The T_c in Ta_2PdS_6 exhibits a drastic enhancement above 80.4 GPa and reaches 11.2 K at 130.0 GPa, which is almost twice the T_c observed in the first dome. In Ta_2PdSe_6 , the emergence of the second dome is also observed above 102.1 GPa. The observed higher T_c in the second dome is motivative for further investigation of fundamental physics in this materials system. Although we consider that the drastic enhancements of T_c in these compounds likely originate from modifications in the electronic structures, challenges remain in conducting structural analysis at the corresponding pressure.

ACKNOWLEDGMENTS

This work was partly supported by JSPS KAKENHI Grant Numbers 23H01835, 23K13549, and 23KK0088. The fabrication process of diamond electrodes was partially supported by the NIMS Nanofabrication Platform in the Nanotechnology Platform Project sponsored by the Ministry of Education, Culture, Sports, Science and Technology (MEXT), Japan. The synchrotron X-ray experiments were performed at AR-NE1A (KEK-PF) under the approval of Proposal No. 2022G049 with support from Dr. Y. Shibasaki (KEK).

References

- [1] K. Matsuura et al., Maximizing T_c by tuning nematicity and magnetism in $\text{FeSe}_{1-x}\text{S}_x$ superconductors, *Nat. Commun.* **8**, 1143 (2017).
- [2] M. Bendele, A. Amato, K. Conder, M. Elender, H. Keller, H.-H. Klauss, H. Luetkens, E. Pomjakushina, A. Raselli, and R. Khasanov, Pressure Induced Static Magnetic Order in Superconducting FeSe_{1-x} , *Phys. Rev. Lett.* **104**, 087003 (2010).
- [3] A. E. Böhmer et al., Distinct pressure evolution of coupled nematic and magnetic orders in FeSe , *Phys. Rev. B* **100**, 064515 (2019).
- [4] G. Wang et al., Pressure-Induced Superconductivity In Polycrystalline $\text{La}_3\text{Ni}_2\text{O}_{7-\delta}$, *Phys. Rev. X* **14**, 011040 (2024).
- [5] S. Sahoo, U. Dutta, L. Harnagea, A. K. Sood, and S. Karmakar, Pressure-induced suppression of charge density wave and emergence of superconductivity in 1T-VSe_2 , *Phys. Rev. B* **101**, 014514 (2020).
- [6] A. F. Kusmartseva, B. Sipoş, H. Berger, L. Forró, and E. Tutiş, Pressure Induced Superconductivity in Pristine 1T-TiSe_2 , *Phys. Rev. Lett.* **103**, 236401 (2009).
- [7] Z. Zhang et al., Pressure-induced reemergence of superconductivity in the topological kagome metal CsV_3Sb_5 , *Phys. Rev. B* **103**, 224513 (2021).
- [8] J. P. Sun et al., Reemergence of high- T_c superconductivity in the $(\text{Li}_{1-x}\text{Fe}_x)\text{OHFe}_{1-y}\text{Se}$ under high pressure, *Nat. Commun.* **9**, 380 (2018).
- [9] L. Sun et al., Re-emerging superconductivity at 48 kelvin in iron chalcogenides, *Nature* **483**, 67 (2012).
- [10] J. Nokelainen, M. E. Matzelle, C. Lane, N. Atlam, R. Zhang, R. S. Markiewicz, B. Barbiellini, J. Sun, and A. Bansil, Second dome of superconductivity in $\text{YBa}_2\text{Cu}_3\text{O}_7$ at high pressure, *Phys. Rev. B* **110**, L020502 (2024).
- [11] M. A. ElGhazali, P. G. Naumov, H. Mirhosseini, V. Süß, L. MÜchler, W. Schnelle, C. Felser, and S. A. Medvedev, Pressure-induced superconductivity up to 13.1 K in the pyrite phase of palladium diselenide PdSe_2 , *Phys. Rev. B* **96**, 060509 (2017).
- [12] Y. Qi et al., Superconductivity in Weyl semimetal candidate MoTe_2 , *Nat. Commun.* **7**, 11038 (2016).
- [13] X.-C. Pan et al., Pressure-driven dome-shaped superconductivity and electronic structural evolution in tungsten ditelluride, *Nat. Commun.* **6**, 7805 (2015).
- [14] A. Nakano, U. Maruoka, F. Kato, H. Taniguchi, and I. Terasaki, Room Temperature Thermoelectric Properties of Isostructural Selenides Ta_2PdS_6 and Ta_2PdSe_6 , *J. Phys. Soc. Jpn.* **90**, 033702 (2021).
- [15] F. Kato, U. Maruoka, A. Nakano, T. Manjo, D. Ishikawa, A. Q. R. Baron, Y. Yasui, T. Hasegawa, and I. Terasaki, Enhanced Cryogenic Thermoelectricity in Semimetal Ta_2PdSe_6 through Non-Fermi Liquid-Like Charge and Heat Transport, *Adv. Phys. Res.* 2400063 (2024).
- [16] H. Yang et al., Pressure-induced superconductivity in quasi-one-dimensional semimetal Ta_2PdSe_6 , *Phys. Rev. Mater.* **6**, 084803 (2022).
- [17] W. Liu, J. Feng, Q. Hou, B. Li, K. Wang, B. Chen, S. Li, and Z. Shi, Pressure-induced superconductivity and isosymmetric structural transition in quasi-one-dimensional Ta_2PdS_6 , *Phys.*

Rev. B **109**, 054513 (2024).

- [18] A. Nakano, U. Maruoka, and I. Terasaki, Correlation between thermopower and carrier mobility in the thermoelectric semimetal Ta₂PdSe₆, *Appl. Phys. Lett.* **121**, 153903 (2022).
- [19] A. Nakano, A. Yamakage, U. Maruoka, H. Taniguchi, Y. Yasui, and I. Terasaki, Giant Peltier conductivity in an uncompensated semimetal Ta₂PdSe₆, *J. Phys. Energy* **3**, 044004 (2021).
- [20] K. Momma and F. Izumi, VESTA 3 for three-dimensional visualization of crystal, volumetric and morphology data, *J. Appl. Crystallogr.* **44**, 1272 (2011).
- [21] R. Matsumoto, Y. Sasama, M. Fujioka, T. Irifune, M. Tanaka, T. Yamaguchi, H. Takeya, and Y. Takano, Note: Novel diamond anvil cell for electrical measurements using boron-doped metallic diamond electrodes, *Rev. Sci. Instrum.* **87**, 076103 (2016).
- [22] R. Matsumoto, T. Irifune, M. Tanaka, H. Takeya, and Y. Takano, Diamond anvil cell using metallic diamond electrodes, *Jpn. J. Appl. Phys.* **56**, 05FC01 (2017).
- [23] R. Matsumoto et al., Pressure-Induced Superconductivity in Sulfur-Doped SnSe Single Crystal Using Boron-Doped Diamond Electrode-Prefabricated Diamond Anvil Cell, *J. Phys. Soc. Jpn.* **87**, 124706 (2018).
- [24] H. K. Mao, P. M. Bell, J. W. Shaner, and D. J. Steinberg, Specific volume measurements of Cu, Mo, Pd, and Ag and calibration of the ruby R1 fluorescence pressure gauge from 0.06 to 1 Mbar, *J. Appl. Phys.* **49**, 3276 (1978).
- [25] Y. Akahama and H. Kawamura, High-pressure Raman spectroscopy of diamond anvils to 250GPa: Method for pressure determination in the multimegabar pressure range, *J. Appl. Phys.* **96**, 3748 (2004).
- [26] Y. Seto, D. Hamane, T. Nagai, and K. Fujino, Fate of carbonates within oceanic plates subducted to the lower mantle, and a possible mechanism of diamond formation, *Phys. Chem. Miner.* **35**, 223 (2008).
- [27] W. L. McMillan, Transition Temperature of Strong-Coupled Superconductors, *Phys. Rev.* **167**, 331 (1968).
- [28] J. Bardeen, L. N. Cooper, and J. R. Schrieffer, Theory of Superconductivity, *Phys. Rev.* **108**, 1175 (1957).
- [29] J. Zhang et al., Observation of two superconducting domes under pressure in tetragonal FeS, *Npj Quantum Mater.* **2**, 49 (2017).
- [30] J. Yang, R. Zhou, L.-L. Wei, H.-X. Yang, J.-Q. Li, Z.-X. Zhao, and G.-Q. Zheng, New Superconductivity Dome in LaFeAsO_{1-x}F_x Accompanied by Structural Transition, *Chin. Phys. Lett.* **32**, 107401 (2015).
- [31] Y. Zhou et al., Pressure-induced reemergence of superconductivity in topological insulator Sr_{0.065}Bi₂Se₃, *Phys. Rev. B* **93**, 144514 (2016).
- [32] S. McDonnell, R. Addou, C. Buie, R. M. Wallace, and C. L. Hinkle, Defect-Dominated Doping and Contact Resistance in MoS₂, *ACS Nano* **8**, 2880 (2014).
- [33] S. Zhang, C.-G. Wang, M.-Y. Li, D. Huang, L.-J. Li, W. Ji, and S. Wu, Defect Structure of Localized Excitons in a WSe₂ Monolayer, *Phys. Rev. Lett.* **119**, 046101 (2017).
- [34] N. R. Werthamer, E. Helfand, and P. C. Hohenberg, Temperature and Purity Dependence of the Superconducting Critical Field, H_{c2} . III. Electron Spin and Spin-Orbit Effects, *Phys. Rev.* **147**,

295 (1966).

- [35] T. Baumgartner, M. Eisterer, H. W. Weber, R. Flükiger, C. Scheuerlein, and L. Bottura, Effects of neutron irradiation on pinning force scaling in state-of-the-art Nb₃Sn wires, *Supercond. Sci. Technol.* **27**, 015005 (2014).
- [36] W. Sano, T. Koretsune, T. Tadano, R. Akashi, and R. Arita, Effect of Van Hove singularities on high- T_c superconductivity in H₃S, *Phys. Rev. B* **93**, 094525 (2016).